Journal of Integrative Neuroscience

J. Integr. Neurosci. **2026**; 25(6): 50669
https://doi.org/10.31083/JIN50669

Original Research

Serpinb2 is Upregulated in Dorsal Root Ganglia and Associated With Neuroinflammatory Changes in a Mouse Model of Neuropathic Pain

Doudou Zhao[1,2,†], Ziye Jia[1,2,†], Ali Zou[1,2], Xinyu Zhang[2], Enjun Lei[1,*]

[1]Department of Anesthesiology, The First Affiliated Hospital of Nanchang University, Jiangxi Medical College, Nanchang University, 330006 Nanchang, Jiangxi, China
[2]The First Clinical Medical College of Nanchang University, 330006 Nanchang, Jiangxi, China
*Correspondence: leienjun@126.com (Enjun Lei)
[†]These authors contributed equally.
Academic Editor: Vincent Lelievre
Submitted: 3 February 2026 Revised: 18 April 2026 Accepted: 22 April 2026 Published: 22 June 2026

Abstract

Background: Neuropathic pain (NP) is a refractory chronic pain condition that severely impairs quality of life, while currently available treatments often provide insufficient relief. Emerging evidence indicates that neuroinflammation in the dorsal root ganglion (DRG) is critically involved in the development and maintenance of NP; however, the molecular mechanisms responsible for this process remain to be elucidated. The aim of this study was to identify and validate key genes involved in NP and to investigate their potential as therapeutic targets. **Methods**: Integrated bioinformatic analyses were performed using multiple DRG transcriptomic datasets derived from a spared nerve injury (SNI) model. Differential expression analysis and weighted gene co-expression network analysis were used to identify NP-associated genes, followed by functional enrichment analyses. Experimental validation was subsequently conducted in an SNI mouse model. Mechanical sensitivity and anxiety-like behaviors were assessed, and the expression of candidate genes in ipsilateral L4–L6 DRGs was examined using quantitative reverse transcription quantitative polymerase chain reaction (RT-qPCR) and immunohistochemistry. **Results**: Eight candidate genes associated with NP were identified through integrated bioinformatic analyses. Among these, serpin family B member 2; plasminogen activator inhibitor-2, PAI-2 (*Serpinb2*) was consistently upregulated across datasets. The well-established pain-related gene sodium voltage-gated channel alpha subunit 3 (*Scn3a*) was included as a reference. *Serpinb2*-associated gene networks were primarily enriched in inflammatory and immune-related pathways. SNI mice developed significant mechanical allodynia and anxiety-like behaviors. Consistent with these findings, *Serpinb2* expression was significantly increased in DRG tissues at both the mRNA and protein levels. **Conclusions**: *Serpinb2* may represent a previously underappreciated molecule associated with DRG neuroinflammation in NP and may serve as a potential target for further investigation.

Keywords: dorsal root ganglia; gene expression profiling; neuralgia; neuroinflammation; peripheral nervous system diseases

1. Introduction

Pain is regarded as a significant public health challenge, second only to cardiovascular and cerebrovascular diseases and cancer in terms of its impact worldwide. Neuropathic pain (NP), a chronic pain state that is difficult to manage, results from damage or disease in the somatosensory nervous system and is thought to comprise about 15–25% of chronic pain conditions worldwide [1]. Compared with other types of pain, NP is characterized by a prolonged disease course, poor therapeutic response, and a high rate of recurrence. Its disease process is very complicated and includes numerous interacting mechanisms, including peripheral and central sensitization, dysfunction of descending inhibitory pathways, ion channel abnormalities, activation of spinal glial cells, and neuroimmune inflammatory responses. Owing to the multidimensional and heterogeneous nature of these mechanisms, a considerable proportion of patients fail to achieve rapid and effective pain relief, leading to a marked reduction in quality of life [2,3].

Current clinical management of NP mainly includes pharmacological and non-pharmacological interventions. Pharmacological treatment mainly includes opioids, antidepressants, ion channel-targeting agents, and non-steroidal anti-inflammatory drugs, while non-pharmacological interventions encompass exercise therapy, ultrasound therapy, shock wave therapy, and pulsed radiofrequency treatment. Although combined treatment strategies can provide partial symptom relief, their clinical utility is still limited by drug dependence, restricted patient eligibility, and unsatisfactory long-term outcomes [4]. Those limitations indicate the urgent need to further elucidate the molecular basis of NP and to identify novel therapeutic targets.

In recent years, with the emergence of the "whole nervous system injury" concept [5,6], accumulating evidence indicates that NP is not simply confined to pain within the distribution of the injured nerve, but instead reflects a complex pathological state accompanied by extensive structural and functional alterations in both the peripheral and central nervous systems. Within this framework, the dorsal root

ganglion (DRG), which represents the first relay node for peripheral sensory input before entry into the central nervous system, is widely regarded as a key site involved in both the onset and maintenance of NP [7].

Recent evidence has indicated that neuroinflammation within the DRG is not simply a passive consequence of nerve injury, but rather an active driving force in pain generation and chronification. In the initial phase after nerve injury, inflammatory factors contribute to the sensitization of DRG sensory neurons and promote the secretion of signaling mediators such as adenosine triphosphate (ATP), colony-stimulating factor 1 (CSF1), chemokines, and proteolytic enzymes. These signals subsequently activate spinal microglia and astrocytes, thereby amplifying inflammatory cascades and enhancing neuronal excitability [8,9]. In addition, several non-pharmacological analgesic interventions, including electroacupuncture and pulsed radiofrequency, have been reported to exert beneficial effects partly through modulation of inflammatory responses in the DRG or spinal dorsal horn [10]. Those findings further support the view that inflammatory regulation within the DRG constitutes an important mechanistic basis and potential therapeutic entry point for NP.

Extensive studies have established ion channels and classical inflammatory mediators as major contributors to NP [10,11,12]. In particular, voltage-gated sodium channels encoded by sodium voltage-gated channel alpha subunit 9 (*Scn9a*) and sodium voltage-gated channel alpha subunit 10 (*Scn10a*), corresponding to Nav1.7 and Nav1.8, respectively, are widely recognized as key determinants of nociceptive transmission and chronic pain [13]. Nevertheless, the molecular landscape of NP is highly context-dependent and may vary across injury paradigms, tissues, and temporal stages [12]. Therefore, transcriptomic profiling of DRG tissue may reveal not only canonical pain-related molecules, but also additional channel subtypes and inflammation-associated genes that are preferentially involved in specific pathological settings. In addition, reliance on a single transcriptomic dataset for key gene screening is susceptible to sample heterogeneity and technical noise, which may reduce the robustness and reproducibility of candidate discovery.

To overcome these limitations, the present study integrated multiple DRG transcriptomic datasets derived from the spared nerve injury (SNI) model, including GSE24982, GSE30691, and GSE63442. We systematically characterized the differential gene expression landscape under NP conditions and identified reproducible molecules potentially involved in disease initiation and maintenance.

By combining integrated bioinformatic screening with molecular and histological validation, this study was designed to identify reproducible DRG-associated molecular alterations in NP and to further characterize the expression pattern and potential significance of serpin family B member 2; plasminogen activator inhibitor-2, PAI-2 (*Serpinb2*) in the DRG under NP conditions. Our intention was to provide new evidence that links *Serpinb2* to neuroimmune regulation and pain maintenance, and offer a novel perspective for understanding the molecular mechanisms underlying NP.

2. Materials and Methods

2.1 Data Preprocessing and Identification of NP-Related Key Genes

Three transcriptomic datasets related to NP, namely GSE24982, GSE30691, and GSE63442, were retrieved from the Gene Expression Omnibus (GEO) database (https://www.ncbi.nlm.nih.gov/geo/). All datasets were generated from DRG tissues obtained from SNI models. Following normalization and $\log_2$ transformation, batch effects across datasets were removed using the ComBat algorithm implemented in the sva package version 3.52.0 in R (Bioconductor, Boston, MA, USA; https://bioconductor.org/packages/sva/). Principal component analysis (PCA) was then applied to evaluate the integration quality. Differentially expressed genes were identified with the limma package (version 3.23, https://bioconductor.org/packages/limma/) using the criteria of $|\log_2$ fold change (FC)$| \geq 0.6$ and false discovery rate (FDR) ≤ 0.05.

2.2 Construction and Identification of NP-Related Co-Expression Modules by WGCNA

To identify co-expression modules significantly associated with NP, weighted gene co-expression network analysis (WGCNA) was independently performed on the GSE24982 and GSE63442 datasets. The top 5000 genes ranked by variance were selected for analysis. An appropriate soft-thresholding power (β) was determined according to the scale-free topology criterion, after which a topological overlap matrix was constructed. Gene modules were identified by hierarchical clustering combined with the dynamic tree-cutting algorithm. Module eigengenes (MEs) were then correlated with phenotypic traits (Control/NP), and modules showing strong associations with NP were defined as key modules.

2.3 Screening and Expression Validation of Key Genes

Genes from key WGCNA modules were overlapped with the differentially expressed genes (DEGs) to identify candidate hub genes. Gene expression differences between the control and NP groups were visualized using violin plots generated with the ggpubr package (version 0.6.3, https://cran.r-project.org/package=ggpubr) in R. Group comparisons were performed using the Wilcoxon rank-sum test, and $p \leq 0.05$ was considered statistically significant.

2.4 Evaluation of the Diagnostic Capabilities of Essential Genes via ROC Curve Analysis

A receiver operating characteristic (ROC) curve analysis was performed with the pROC R package (ver-

sion 1.19.0.1, https://cran.r-project.org/package=pROC) to evaluate how well key genes can distinguish NP samples from control samples. The area under the curve (AUC), along with the optimal cutoff value, sensitivity, and specificity, was computed. An AUC above 0.8 was considered to reflect good diagnostic capability.

2.5 Co-Expression Pattern Analysis

Eight key genes with prominent performance in the ROC analysis, including C-C motif chemokine receptor 5 (*Ccr5*), contactin-associated protein 1 (*Cntnap1*), DLG-associated protein 3 (*Dlgap3*), high mobility group box 2 (*Hmgb2*), *Loc102545839*, defensin RatNP-3 precursor (*Ratnp-3b*), *Scn3a* and *Serpinb2*, were selected as core genes. Pearson correlation coefficients were calculated between these genes and all other genes. Co-expressed genes meeting the criteria of $|r| \geq 0.6$ and $p \leq 0.05$ were retained, and their expression patterns and clustering features were visualized using heatmaps generated with the pheatmap R package (version 1.0.13, https://cran.r-project.org/package=pheatmap).

2.6 Correlation Analysis of Key Genes

The corrplot R package (version 0.95, https://cran.r-project.org/package=corrplot) was used to calculate the correlation matrix of the eight key genes and their co-expressed genes. The screening thresholds were set at $|r| \geq 0.6$ and $p \leq 0.05$.

2.7 Gene Ontology (GO) Analysis for Functional Enrichment

GO enrichment analysis was conducted for the eight key genes and their co-expressed genes using the clusterProfiler package in R, encompassing the three principal GO domains: biological process (BP), cellular component (CC), and molecular function (MF). Adjusted *p* values were calculated using the Benjamini–Hochberg method, and *p*.adjust ≤ 0.05 was considered statistically significant.

2.8 Analysis of Kyoto Encyclopedia of Genes and Genomes (KEGG) Pathway Enrichment

The same gene set underwent KEGG pathway enrichment analysis using the clusterProfiler R package (version 3.23, https://bioconductor.org/packages/clusterProfiler/), where *p*.adjust ≤ 0.05 was regarded as statistically significant.

2.9 Analysis of Gene Set Enrichment (GSEA)

To assess the potential regulatory relevance of the key genes in NP, samples were classified into high- and low-expression groups according to the expression of each of the eight key genes. GSEA was performed using the clusterProfiler and enrichplot packages (version 3.23, https://bioconductor.org/packages/enrichplot/) with the KEGG gene set (c2.cp.kegg.v7.5.1.symbols.gmt) as the reference. A total of 1000 permutations were conducted, and significance was defined as *p*.adjust ≤ 0.05 and $|NES| > 1$.

2.10 Animals and Surgery

Male wild-type C57BL/6 mice (6–8 weeks old) were purchased from Jiangsu Jicui Yaokang Biotechnology Co., Ltd (Nanjing, Jiangsu, China). Animals were housed in groups of 5 per cage in individually ventilated cages (IVCs; 365 × 207 × 140 mm, length × width × height; floor area ~530 cm^2) at the animal facility of The First Affiliated Hospital of Nanchang University. Housing conditions were controlled at 20–24 °C with 40–60% humidity under a 12 h light/dark cycle, and food and water were provided ad libitum. Bedding was replaced every 3 days.

The SNI model was established in the right hindlimb under sterile conditions as previously described by Decosterd and Woolf [14,15]. Mice were anesthetized with inhaled isoflurane, induced in an induction chamber with 3%–5% isoflurane (R510-22-10, RWD Life Science, Shenzhen, Guangdong, China), and subsequently maintained via a nose cone with 1.5%–2.0% isoflurane in oxygen. During surgery, body temperature was maintained with a thermostatically controlled heating pad, and the depth of anesthesia was monitored by respiratory rate, muscle tone, and foot-withdrawal reflex. After adequate anesthesia was achieved, a lateral skin incision was made in the right hindlimb. The muscles were carefully separated to reveal the three end branches of the sciatic nerve: the tibial nerve, the common peroneal nerve, and the sural nerve. The tibial and common peroneal nerves were firmly tied with 6-0 silk sutures, using two ties for each nerve, and then cut between the tied areas to stop nerve regrowth, while the sural nerve remained untouched. The nerve stumps were then repositioned to their original anatomical locations.

Erythromycin ophthalmic ointment (H36020018, Renhe Pharmaceutical Co., Ltd., Nanchang, Jiangxi, China) was applied to the muscle layer, after which the muscles were repositioned and the skin was sutured. The ointment was reapplied postoperatively to prevent infection. In Sham group, the surgical procedure was identical, except the nerves were neither tied nor severed, and they were housed separately from the SNI mice after the surgery.

2.11 Behavioral Testing

Behavioral tests were conducted between 07:00 and 19:00, during the light phase. To reduce potential order effects, the testing order was counterbalanced among mice, and at least 24 h was allowed between successive behavioral assessments. Von Frey filaments were used to assess mechanical sensitivity, while anxiety-like behaviors were evaluated through the elevated plus maze (EPM) and open field test (OFT). To minimize subjective bias and improve data reliability, behavioral assessments were conducted in a blinded manner: one investigator who was aware of the

group allocation placed the mice in the testing environment, whereas a second investigator who was blinded performed the behavioral testing and data collection.

Mechanical sensitivity test: Mechanical sensitivity was measured using von Frey filaments (NC12775, North Coast Medical, Morgan Hill, CA, USA) according to the up–down paradigm [16,17]. Graded mechanical stimuli were applied to the plantar surface of the hind paw, and the paw withdrawal mechanical threshold (PWMT) was calculated and expressed in grams (g).

OFT test: Spontaneous locomotor activity and anxiety-like behavior were evaluated using the OFT in a transparent square chamber (50 × 50 × 40 cm). A central area measuring 25 × 25 cm was predefined for analysis. Testing was conducted 1 day before SNI surgery and repeated on postoperative day 28. At the start of each session, each mouse was individually introduced into the center of the apparatus and permitted to explore freely for 15 min under dim illumination. Animal movement was recorded throughout the session and analyzed using an automated tracking system (Any-Maze V7.49, Stoelting Co., Wood Dale, IL, USA). The proportion of time spent in the central zone, total distance traveled, and mean locomotor speed were used as outcome measures. To minimize potential interference from olfactory residues, the arena was cleaned with 75% ethanol and allowed to dry completely between trials.

EPM test: Anxiety-like behavior was assessed using the EPM, which consisted of two opposing open arms and two opposing enclosed arms (each 44 × 12 cm) connected by a central square platform (12 × 12 cm). The apparatus was positioned 50 cm above the floor. Behavioral testing was performed 1 day before SNI surgery and again on postoperative day 28. At the beginning of each session, each mouse was placed individually on the central platform with its head oriented toward one of the open arms and allowed to explore freely for 5 min. Animal behavior was recorded and analyzed using the Any-Maze tracking system. The duration spent in the open arms was quantified as indices of anxiety-like behavior. To eliminate possible olfactory interference, the maze was wiped with 75% ethanol and allowed to dry completely between trials.

2.12 Reverse Transcription Quantitative Polymerase Chain Reaction (RT-qPCR)

Total RNA extraction from DRG tissues was performed using TRIzol reagent (15596026CN, Invitrogen, Carlsbad, CA, USA) in accordance with the manufacturer's guidelines. To eliminate genomic DNA contamination and synthesize first-strand cDNA, the HiScript® II 1st Strand cDNA Synthesis Kit (+gDNA wiper) (R212-01, Vazyme Biotech Co., Ltd., Nanjing, Jiangsu, China) was used according to the manufacturer's instructions. Briefly, genomic DNA removal was first performed in a 0.2 mL RNase-free microcentrifuge tube containing 4 µL of 4 × gDNA Wiper Mix, 1 µL of Oligo (dT)23VN (50 µM), 1 µL of random hexamers (50 ng/µL), 1 µL of total RNA, and RNase-free ddH_2O to a final volume of 16 µL. The mixture was briefly centrifuged and incubated at 42 °C for 2 min. First-strand cDNA was then synthesized by adding 2 µL of 10 × RT Mix and 2 µL of HiScript II Enzyme Mix to the above reaction system. After brief centrifugation, reverse transcription was carried out at 50 °C for 15 min, followed by 85 °C for 2 min, and then held at 4 °C. The resulting cDNA concentration was measured using a NanoDrop 2000 spectrophotometer (Thermo Scientific, Waltham, MA, USA) and used for subsequent quantitative analysis.

RT-qPCR was performed on a LightCycler 96 qPCR System (05815916001, Roche, Basel, Switzerland) using 2 × ChamQ Universal SYBR qPCR Master Mix (0711-02, Vazyme, Nanjing, Jiangsu, China). Gene-specific primers for *Serpinb2* (QM18978S), *Scn3a* (QM20690S), *Ccr5* (QM01922S), *Hmgb2* (QM48118S), and *Dlgap3* (QM63142S) were purchased from Beyotime (Shanghai, China). Each qPCR reaction was assembled in a final volume of 10 µL, with 5 µL of 2 × ChamQ Universal SYBR qPCR Master Mix, 0.4 µL of primer pair, 1 µL of template DNA/cDNA, and RNase-free ddH_2O added to reach the desired volume. The amplification program was as follows: initial denaturation at 95 °C for 30 s; followed by 40 cycles of denaturation at 95 °C for 10 s and annealing/extension at 60 °C for 30 s. Melt curve analysis was then performed at 95 °C for 15 s, 60 °C for 60 s, and 95 °C for 15 s. Actb served as the endogenous control, and relative mRNA expression was determined using the $2^{-\Delta\Delta Ct}$ method. Briefly, ΔCt was calculated by subtracting the Ct value of Actb from that of the target gene, whereas $\Delta\Delta$Ct was obtained by comparing the ΔCt of the experimental group with that of the control group. All quantitative experiments were performed with 4 independent replicates to ensure the reliability of the results.

2.13 Immunohistochemistry

For immunohistochemical analysis, 5 mice/group were used in the Sham and SNI groups. Mice were deeply anesthetized with tribromoethanol (T48402, Dalian Meilun Biotechnology, Dalian, Liaoning, China; 250 mg/kg, i.p.), administered as a 1.25% working solution at 20 mL/kg body weight. After adequate anesthesia was established,euthanasia (by transcardial perfusion) was performed via the ascending aorta, first with 0.9% saline and then with freshly prepared 4% paraformaldehyde (R37814, Sigma-Aldrich, St. Louis, MO, USA) in phosphate-buffered saline (PBS, pH 7.4) for tissue fixation. Ipsilateral lumbar dorsal root ganglia (L4–L6) corresponding to the nerve injury were rapidly dissected, fixed in 4% paraformaldehyde for 24 h, routinely paraffin-embedded, and serially sectioned at a thickness of 4 µm.

Paraffin sections were first deparaffinized with xylene (Xilong Scientific Co., Ltd., Shantou, Guangdong, China)

and then rehydrated through a graded ethanol series. Antigen retrieval was subsequently carried out by heat treatment in citrate buffer (pH 6.0; ab64214, Abcam, Cambridge, UK). Endogenous peroxidase activity was quenched using 3% hydrogen peroxide (88597, Millipore, Burlington, MA, USA), after which the sections were incubated with normal goat serum (C0265, Beyotime Biotechnology) at room temperature for blocking.

Sections were incubated overnight at 4 °C with primary antibodies against *Serpinb2* (rabbit polyclonal, 1:500; TA5174S, ABMART, Shanghai, China) and *Scn3a* (rabbit polyclonal, 1:500; PC12133S, ABMART). The following day, sections were incubated at room temperature with an HRP-conjugated goat anti-rabbit secondary antibody [UltraPolymer Goat anti-Rabbit IgG (H&L)-HRP, RGAR011, Proteintech, Wuhan, Hubei, China] at a dilution ratio of 1:500. The visualization of immunoreactivity was achieved with 3,3′-diaminobenzidine (91-95-2, Xilong Scientific Co., Ltd.), and the nuclei were counterstained using hematoxylin (C0107, Beyotime Biotechnology). Whole-slide images were captured using a digital slide scanner (Pannoramic 250 FLASH, 3DHISTECH, Budapest, Hungary) after the processes of dehydration, clearing, and coverslipping. Immunohistochemical staining was quantitatively analyzed using ImageJ 1.54f (National Institutes of Health, Bethesda, MD, USA), with the average optical density of positively stained areas used as the quantitative index.

2.14 Statistical Analysis

All statistical analyses were performed in R. Batch effects across datasets were corrected using the ComBat algorithm in the sva package (sva package version 3.52.0, Bioconductor, Boston, MA, USA. https://bioconductor.org/packages/sva/) and evaluated by PCA. Differential expression analysis was conducted with limma using $|\log_2 FC| \geq 0.6$ and false discovery rate (FDR) <0.05, with p values adjusted by the Benjamini–Hochberg method. In WGCNA, module–trait associations were assessed by Pearson correlation. Group comparisons were performed using the Wilcoxon rank-sum test. ROC analysis was conducted with pROC R package, and AUCs with 95% confidence intervals were calculated. Functional enrichment analyses, including GO and KEGG, were performed using clusterProfiler with p.adjust < 0.05. GSEA was conducted with 1000 permutations, and significance was defined as p.adjust < 0.05 and |NES| >1. Data from behavioral tests, RT-qPCR, and immunohistochemistry are presented as mean ± SEM. All tests were two-tailed, and $p < 0.05$ was considered statistically significant.

3. Results

3.1 Bioinformatics Analysis Reveals Differentially Expressed Genes Associated With NP

After batch effect correction (Fig. 1A,B), PCA demonstrated improved clustering consistency across datasets, indicating effective batch effect removal (**Supplementary Fig. 1**). Differential expression analysis of the integrated datasets identified multiple genes that were significantly altered in NP samples, including the upregulated genes *Scn3a*, *Serpinb2*, *Fc gamma receptor IIa* (*Fcgr2a*), and matrix metallopeptidase 3 (*Mmp3*), and the downregulated genes chromogranin A (*Chga*), 5-hydroxytryptamine receptor 1D (*Htr1d*), and *Cntnap1*.

Heatmap analysis showed clear separation between NP and control samples based on DEG expression patterns (Fig. 1C). The volcano plot further indicated that upregulated genes were mainly associated with inflammatory signaling, extracellular-matrix remodeling, and ion-channel regulation, whereas downregulated genes were primarily related to synaptic transmission and inhibitory neurotransmission (Fig. 1D). Together, these findings indicated that the transcriptomic landscape of NP was characterized by both neuroinflammatory activation and alterations in neuronal function.

3.2 Identification of NP–Related Gene Modules

WGCNA was independently performed on the GSE24982 and GSE63442 datasets to identify gene modules associated with NP. In GSE24982, a soft-thresholding power of $\beta = 8$ achieved an approximately scale-free topology ($R^2 \approx 0.9$) and identified six distinct gene modules (Fig. 2A,C,E). Among them, the brown module showed the strongest negative correlation with NP status ($r = -0.87$, $p = 2 \times 10^{-13}$), whereas the turquoise module showed a significant positive correlation.

In GSE63442, a soft-thresholding power of $\beta = 9$ yielded an optimal network structure ($R^2 > 0.85$) and identified three major modules (Fig. 2B,D,F). The turquoise module displayed an almost perfect positive correlation with NP status ($r = 0.99$, $p = 5 \times 10^{-11}$). These reproducible NP-associated modules across independent datasets provided a robust basis for subsequent key gene screening.

3.3 Immune Inflammation- and Synaptic-Plasticity-Related Genes Showed Distinct Expression Patterns in NP Samples

By intersecting differentially expressed genes with hub genes derived from NP-associated WGCNA modules, eight key genes were identified: *Ccr5*, *Cntnap1*, *Dlgap3*, *Hmgb2*, *Loc102545839*, *Ratnp-3b*, *Scn3a*, and *Serpinb2*. Among these genes, *Ccr5*, *Hmgb2*, *Loc102545839*, *Ratnp-3b*, *Scn3a*, and *Serpinb2* were significantly upregulated in NP samples compared with control samples, whereas *Cntnap1* and *Dlgap3* were significantly downregulated ($p < 0.001$; Fig. 3A–H).

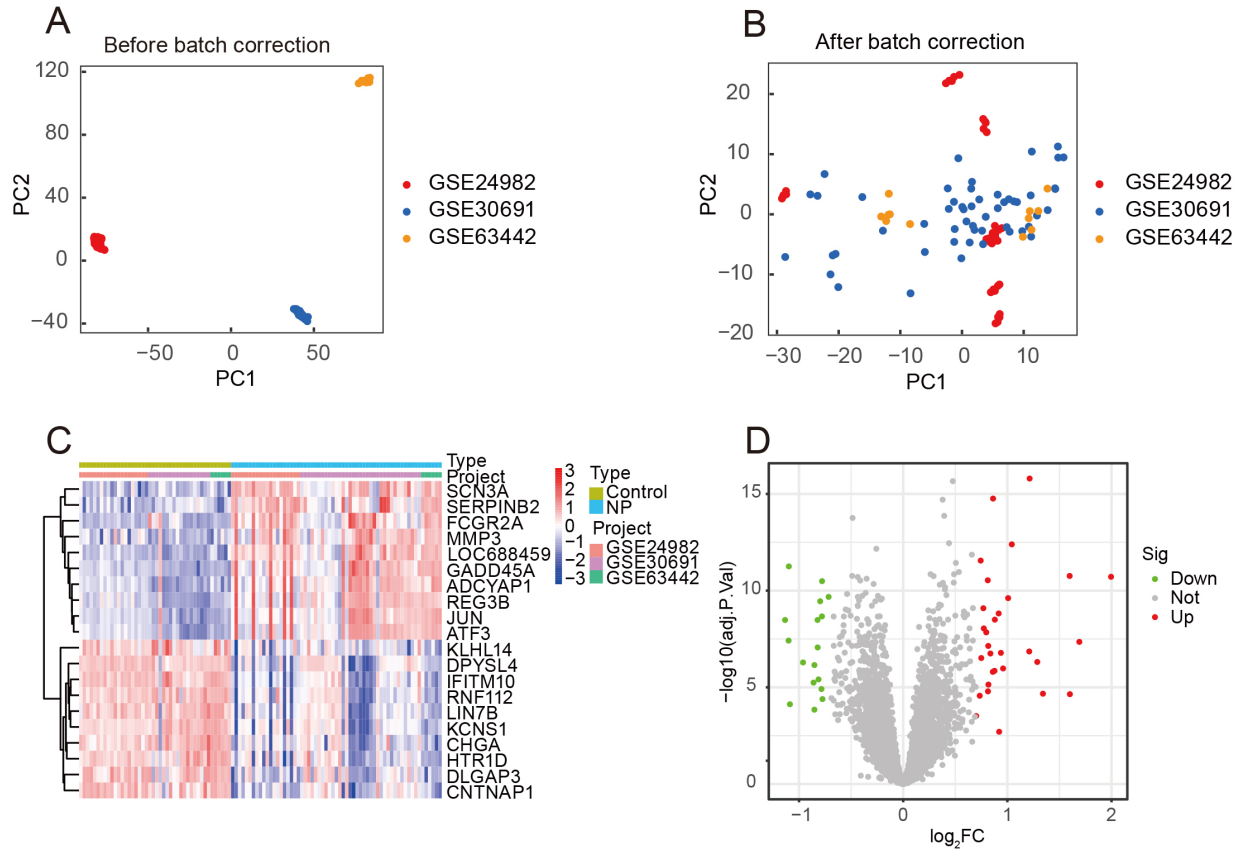

Fig. 1. Incorporating neuropathic pain (NP) transcriptomic data and evaluating genes that show differential expression. (A) Principal component analysis (PCA) before batch correction showing significant batch effects among GSE24982, GSE30691, and GSE63442. (B) PCA after batch correction demonstrating a more consistent sample distribution, indicating that batch effects were effectively removed. (C) Heatmap of differentially expressed genes (DEGs) within the unified dataset. Rows indicate genes, columns indicate samples; red represents genes with elevated expression, and blue represents genes with reduced expression. (D) Volcano plot of DEGs from the merged dataset displays genes with significant upregulation (red) and downregulation (green), and gray dots signify genes without notable changes. ($|\log_2 FC| \geq 0.6$, false discovery rate (FDR) ≤ 0.05).

Functionally, these genes were mainly associated with immune regulation, synaptic organization, and neuronal excitability. Notably, *Serpinb2* was markedly upregulated and showed a strong association with inflammatory signaling and extracellular matrix-related processes, suggesting its potential involvement in NP-associated neuroinflammation.

3.4 Immune Inflammation- and Synaptic-Plasticity-Related Genes Exhibited Strong Diagnostic Performance in NP Samples

ROC curve analysis demonstrated that all eight key genes had discriminative value for distinguishing NP samples from control samples, regardless of whether their expression levels were increased or decreased in NP (Fig. 4A–H). Among them, *Scn3a* (AUC = 0.931) and *Serpinb2* (AUC = 0.875) exhibited the highest diagnostic performance. *Cntnap1* and *Dlgap3* also displayed strong predictive value, whereas *Ccr5* and *Ratnp-3b* showed moderate discriminative ability. These findings suggested that the identified genes, particularly *Serpinb2*, may serve as potential molecular indicators of NP status.

3.5 Co-Expression of NP Key Genes With Immune Inflammation- and Synaptic-Plasticity-Related Pathway Genes

Co-expression analysis revealed that each key gene exhibited distinct yet partially overlapping co-expression patterns with genes involved in immune responses and synaptic regulation (Fig. 5A–H). *Serpinb2* showed significant co-expression with genes related to extracellular matrix remodeling and tissue repair, including Ankyrin Repeat Domain 1 (*Ankrd1*), suggesting its potential association with post-injury inflammatory remodeling.

Other key genes, such as *Scn3a* and *Cntnap1*, were predominantly co-expressed with genes involved in ion channel activity and synaptic signaling, whereas *Ccr5* and *Hmgb2* were more closely associated with immune-related gene clusters.

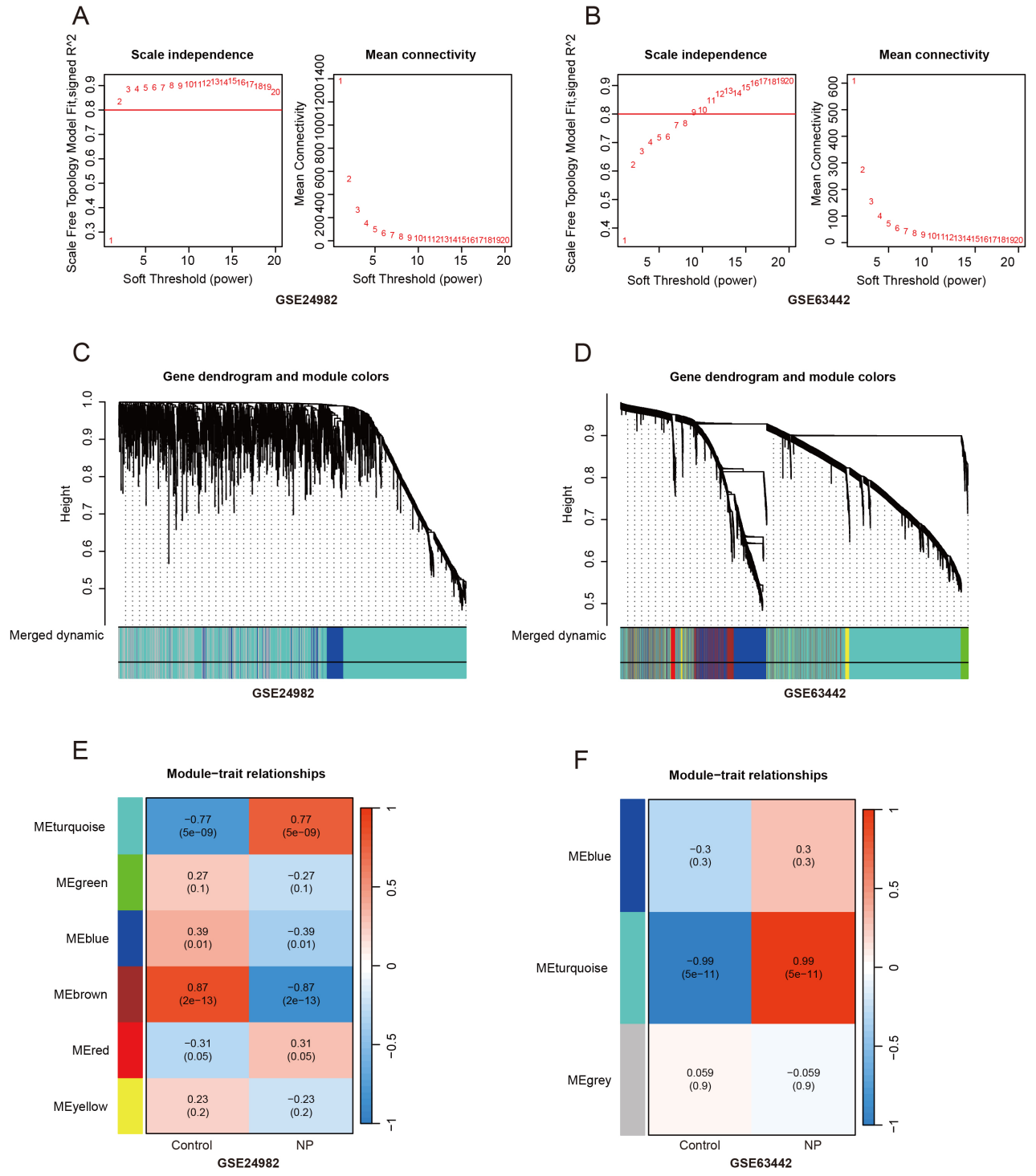

Fig. 2. Weighted gene co-expression network analysis (WGCNA) of NP–related genes. (A,C,E) WGCNA results based on the GSE24982 dataset: (A) Scale-free topology fit index and mean connectivity curves under different soft-thresholding powers; (C) Gene clustering dendrogram and module identification, with different colors representing distinct modules; (E) Heatmap showing correlations between module eigengenes and the NP phenotype (positive correlations are shown in red and negative correlations in blue). (B,D,F) WGCNA results based on the GSE63442 dataset: (B) Soft-threshold selection curves used to determine the optimal β value for constructing a stable network; (D) Visualization of the gene clustering dendrogram and module assignment; (F) Correlation matrix between modules and the NP phenotype, showing a significant positive correlation between the turquoise module and pain status.

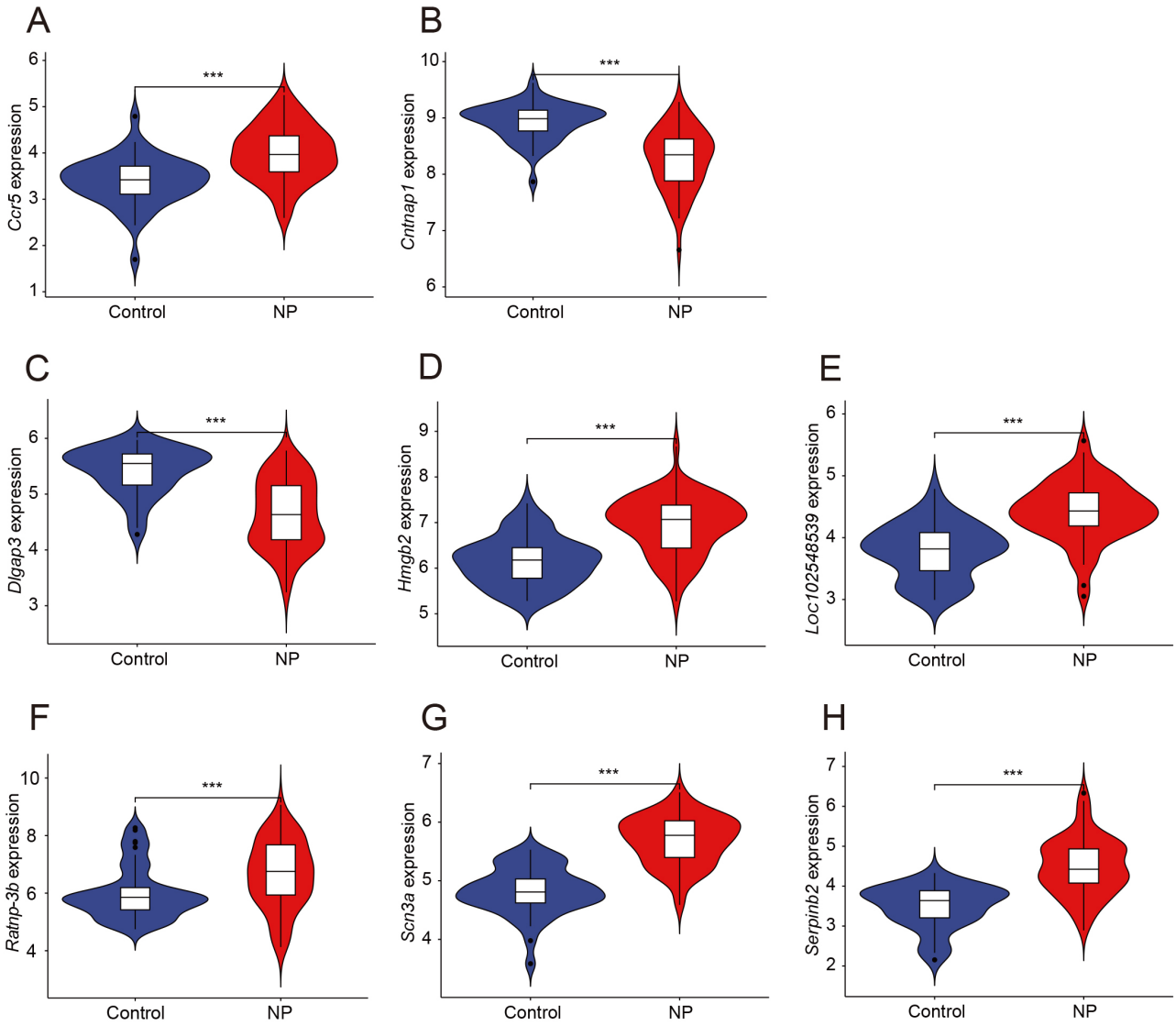

Fig. 3. Expression analysis of key differential genes in NP. Violin plots (A–H) illustrating the expression variations of crucial genes between the NP group (NP, red) and the control group (Control, blue). (A) C-C motif chemokine receptor 5 (*Ccr5*) ($p = 8.39 \times 10^{-7}$); (B) contactin-associated protein 1 (*Cntnap1*) ($p = 4.50 \times 10^{-10}$); (C) DLG-associated protein 3 (*Dlgap3*) ($p = 1.18 \times 10^{-9}$); (D) high mobility group box 2 (*Hmgb2*) ($p = 1.10 \times 10^{-8}$); (E) *LOC102545839* ($p = 2.72 \times 10^{-9}$); (F) defensin RatNP-3 precursor (*Ratnp-3b*) ($p = 0.000893932$); (G) sodium voltage-gated channel alpha subunit 3 (*Scn3a*) ($p = 4.70 \times 10^{-13}$); (H) serpin family B member 2 (*Serpinb2*) ($p = 2.62 \times 10^{-10}$). *Ccr5*, *Hmgb2*, *Loc102545839*, *Ratnp-3b*, *Scn3a*, and *Serpinb2* were significantly upregulated in NP samples compared with control samples, whereas *Cntnap1* and *Dlgap3* were significantly downregulated (***$p < 0.001$).

3.6 NP Key Genes Exhibited Network-Associated Characteristics With Immune Response- and Neuroinflammation-Related Genes

Correlation analysis revealed strong expression relationships between the key genes and their associated gene networks (Fig. 6A–H). *Serpinb2* showed significant positive correlations with several inflammation- and tissue repair-related genes, including *Hmgb2* and *Ankrd1*, further supporting its potential role in neuroinflammatory regulation.

In addition, *Scn3a* was strongly correlated with multiple ion channel-related genes, whereas *Hmgb2* and *Ccr5* were more closely associated with immune and metabolic regulators. These network-level associations further indicated that NP-related key genes may participate in interconnected regulatory programs involving neuroinflammation, immune responses, and neuronal functional regulation.

3.7. GO Functional Enrichment Analysis of NP Key Genes

GO enrichment analysis revealed that the primary genes and their co-expressed partners were significantly in-

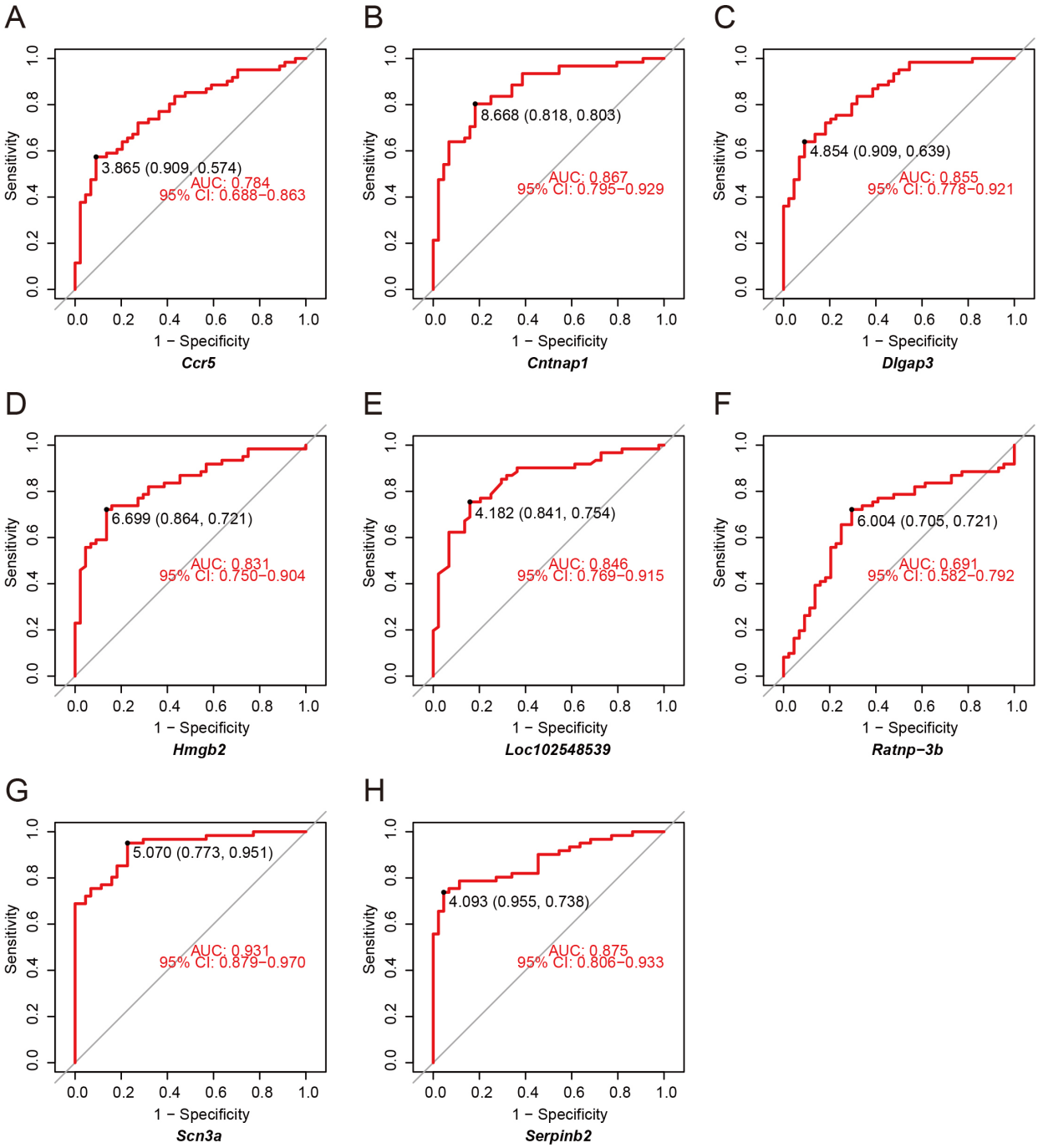

Fig. 4. Receiver operating characteristic (ROC) analysis of the diagnostic performance of key differential genes in NP. (A–H) ROC curves showing the ability of different genes to distinguish the NP group from the control group: (A) *Ccr5*; (B) *Cntnap1*; (C) *Dlgap3*; (D) *Hmgb2*; (E) *Loc102545839*; (F) *Ratnp-3b*; (G) *Scn3a*; (H) *Serpinb2*. The red curves represent the model-fitting results, and the gray dashed diagonal line indicates no discriminative ability, with an area under the curve (AUC) value of 0.5. An AUC value closer to 1 indicates better diagnostic performance. The annotated values represent the optimal cutoff point, sensitivity, specificity, and 95% confidence interval, respectively.

volved in biological processes associated with neural signal transmission, inflammatory responses, ion channel activity, and cytoskeletal organization (Fig. 7A–H). Specifically, genes co-expressed with *Serpinb2* were enriched in muscle processes muscle contraction, sarcomere/myofibril organization, and cation/ligand-gated ion channel activity, suggesting its potential involvement in structural remodeling and cellular stress responses after nerve injury.

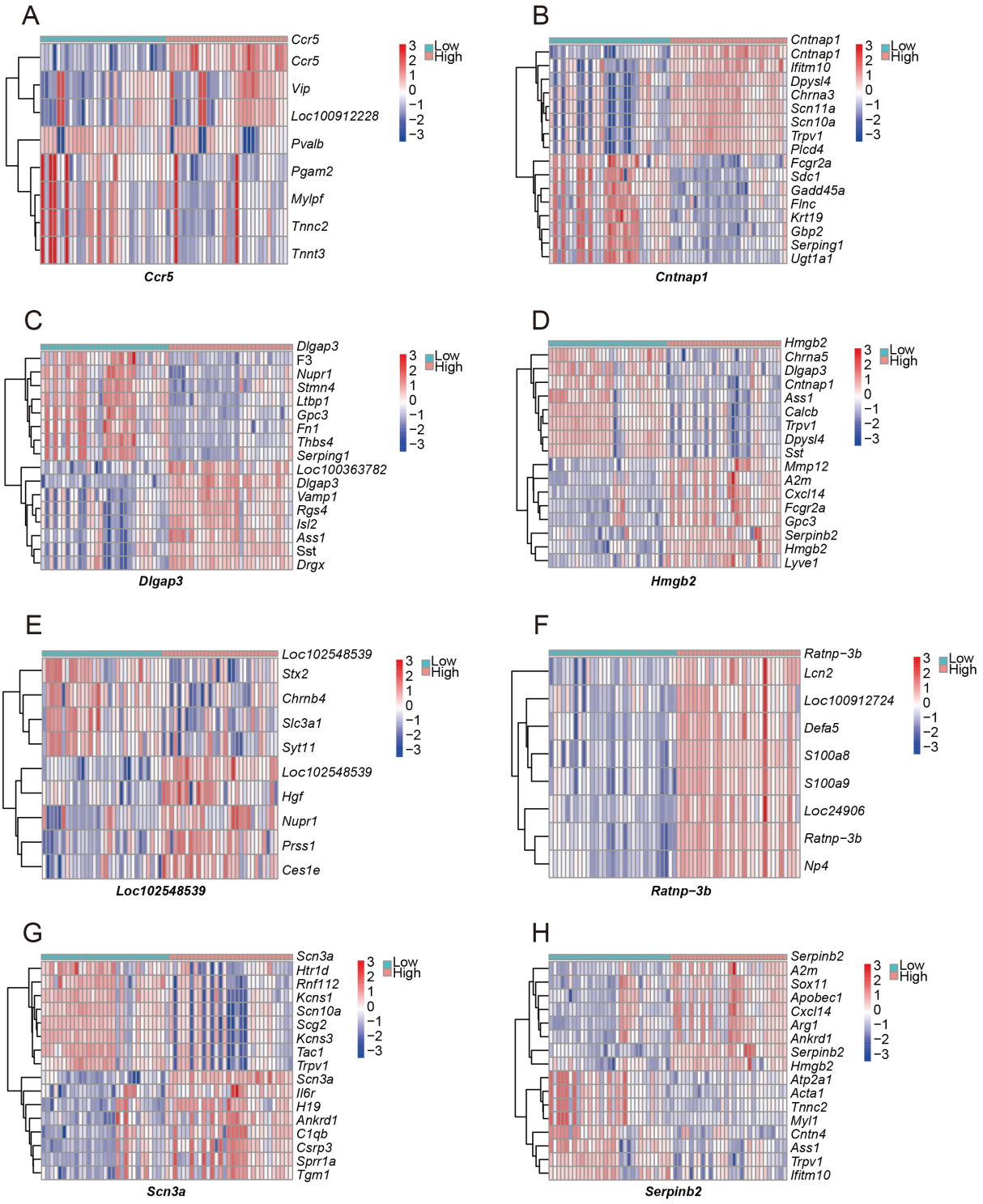

Fig. 5. Co-expression pattern analysis of key genes in NP. (A–H) Heatmap analysis showing the co-expression patterns of eight key genes and their significantly co-expressed genes. (A) *Ccr5*; (B) *Cntnap1*; (C) *Dlgap3*; (D) *Hmgb2*; (E) *Loc102545839*; (F) *Ratnp-3b*; (G) *Scn3a*; (H) *Serpinb2*. Genes with higher expression levels are marked in red, and those with lower levels are marked in blue. Samples are displayed according to the NP group and the control group.

3.8 Enrichment Analysis of KEGG Pathways Related to NP Key Genes

According to KEGG enrichment analysis, NP-related genes were mainly enriched in signaling pathways associated with neuroactive ligand–receptor interaction, complement and coagulation cascades, immune signaling, and metabolic regulation (Fig. 8A–H). Notably, *Serpinb2*-related gene networks were enriched in amino

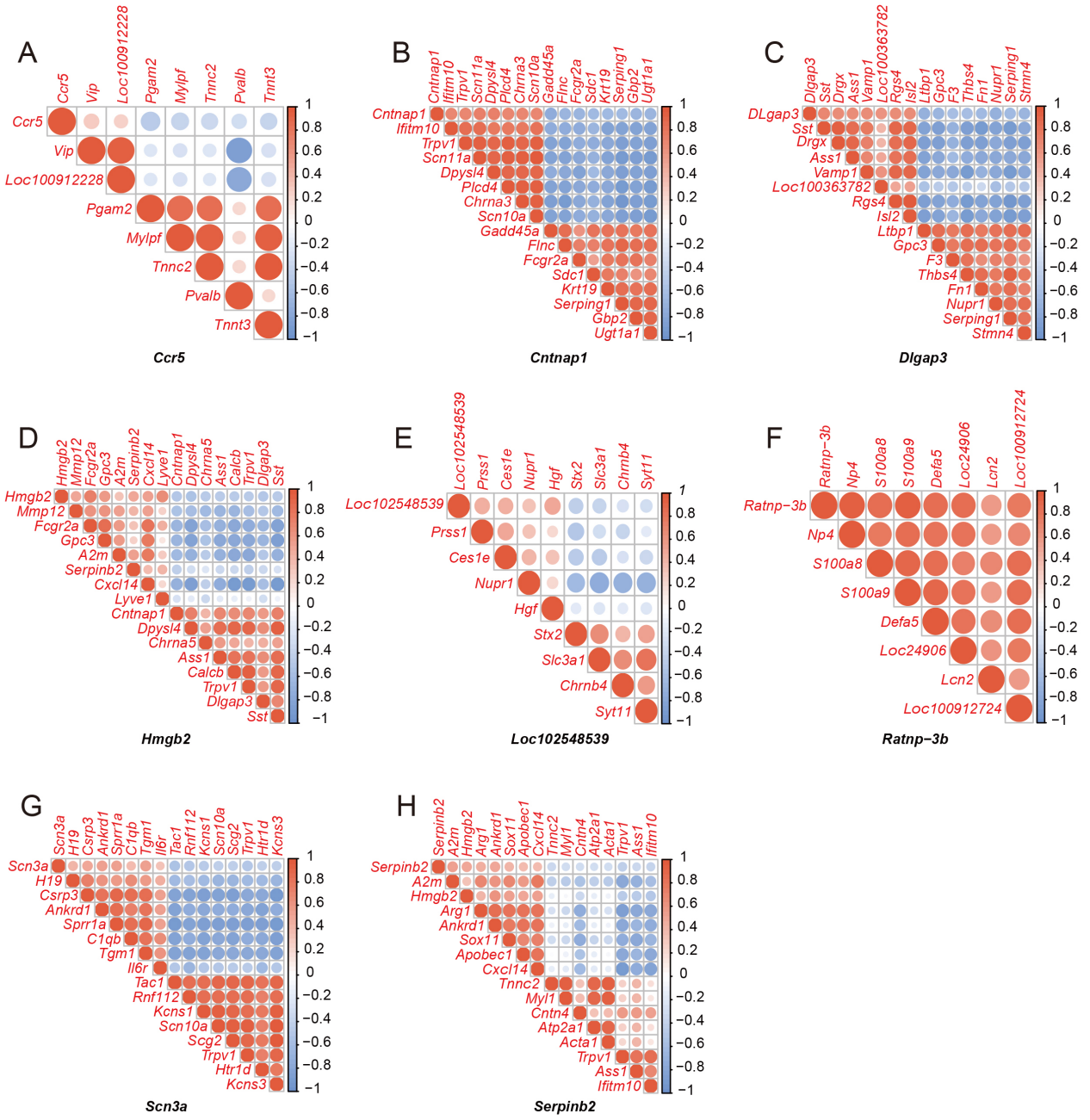

Fig. 6. Correlation analysis of NP key genes and their co-expressed genes. (A–H) Pearson correlation analysis between the eight key genes and their co-expressed genes. (A) *Ccr5*; (B) *Cntnap1*; (C) *Dlgap3*; (D) *Hmgb2*; (E) *Loc102545839*; (F) *Ratnp-3b*; (G) *Scn3a*; (H) *Serpinb2*. Each circle indicates the correlation between two genes; red means a positive correlation, blue means a negative correlation, and the circle's size shows the correlation's intensity.

acid metabolism and cytoskeleton-related pathways, which is consistent with its potential roles in inflammation-associated tissue remodeling and metabolic adaptation.

3.9 GSEA Enrichment Analysis of NP Key Genes

According to GSEA, the important genes were significantly connected with pathways involved in immune activation, inflammatory signaling, neuronal transmission, and energy metabolism (Fig. 9A–H). In particular, the low-expression *Serpinb2* group was enriched in pathways related to protein phosphorylation, muscle contraction, and metabolic processes, suggesting that altered *Serpinb2* expression may reflect changes in cellular stress responses and tissue repair mechanisms in NP.

3.10 Validation of Key Genes in the SNI Mouse Model

Behavioral assessments confirmed the successful establishment of NP after SNI, as indicated by significantly

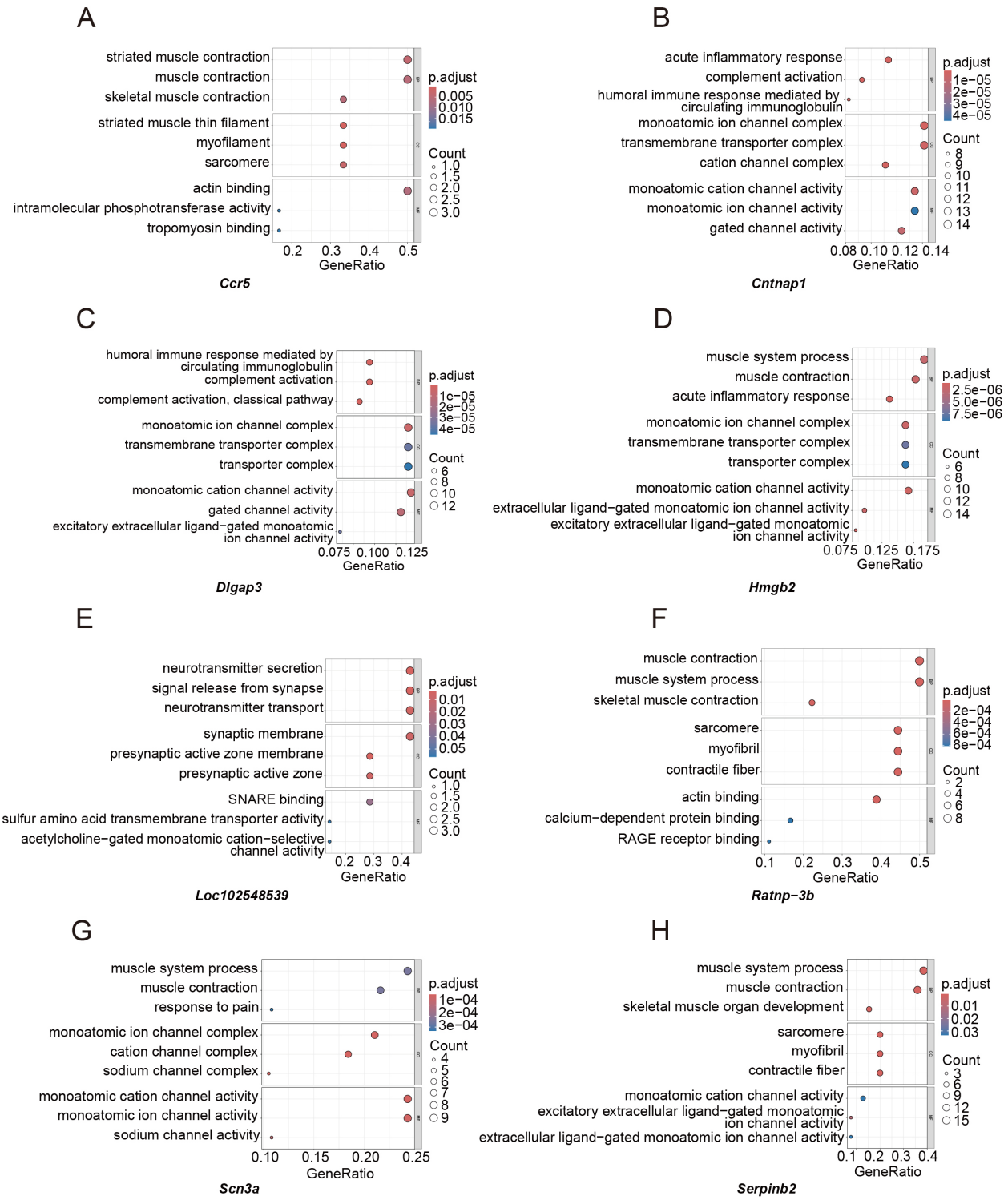

Fig. 7. Gene ontology (GO) functional enrichment analysis of NP key genes and their co-expressed genes. (A–H) Bubble plots showing the GO enrichment results of the eight key genes (*Ccr5, Cntnap1, Dlgap3, Hmgb2, Loc102545839, Ratnp-3b, Scn3a* and *Serpinb2*) and their co-expressed genes. The x-axis represents the GeneRatio, which indicates the proportion of input genes enriched in a given functional category or pathway, and the y-axis indicates significantly enriched GO terms. Bubble size corresponds to the number of enriched genes, and color intensity reflects the significance level (*p*.adjust value).

lower mechanical withdrawal thresholds ($p < 0.0001$) (Fig. 10A,B). Moreover, relative to Sham group, the SNI group spent less time in the central area ($p = 0.0049$) and showed a shorter total travel distance ($p = 0.0251$) in the OFT (Fig.

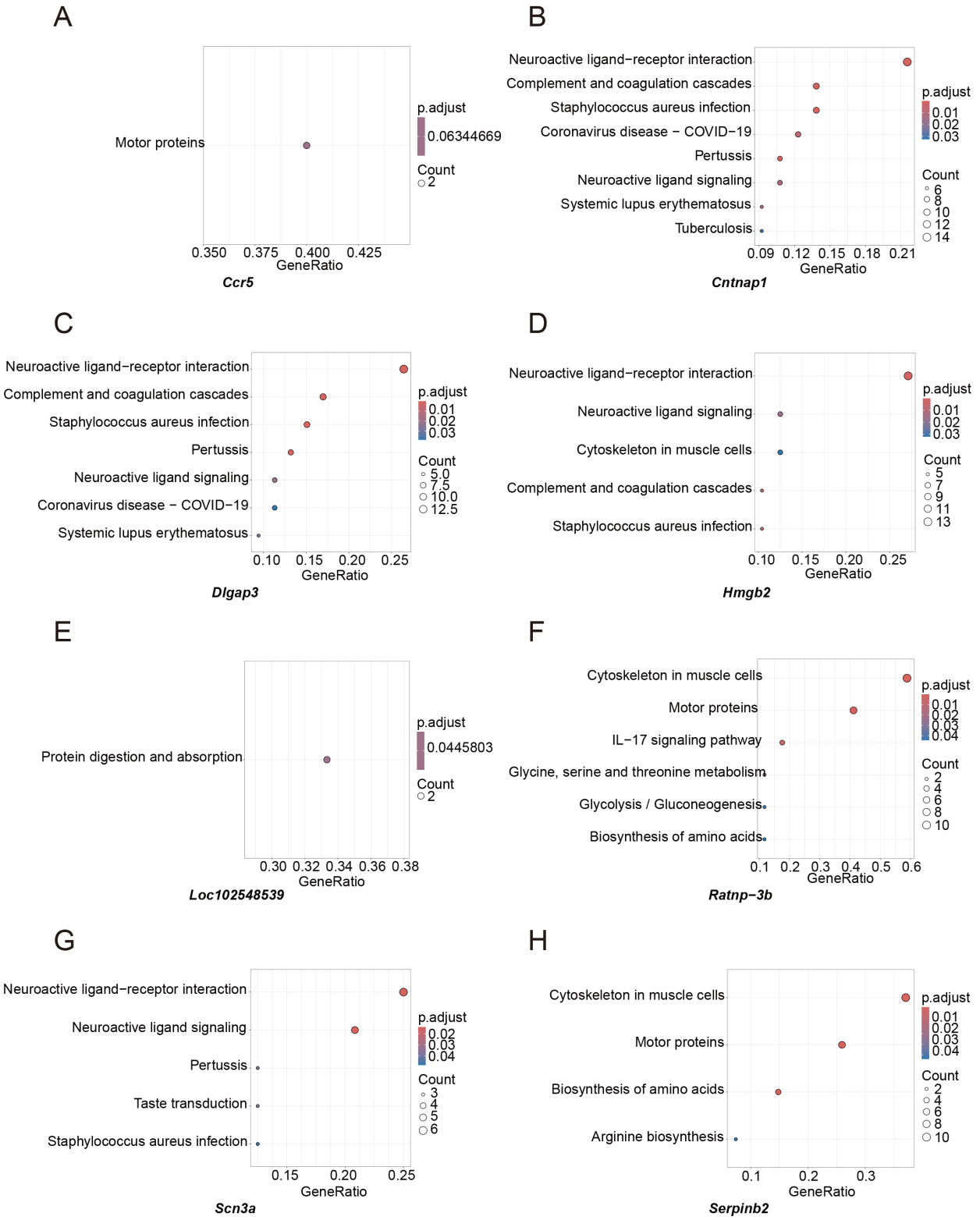

Fig. 8. Kyoto Encyclopedia of Genes and Genomes (KEGG) pathway enrichment analysis of NP key genes and their co-expressed genes. (A–H) Bubble plots showing the KEGG pathway enrichment results of the eight key genes (*Ccr5, Cntnap1, Dlgap3, Hmgb2, Loc102545839, Ratnp-3b, Scn3a and Serpinb2*) and their co-expressed genes. The x-axis represents the GeneRatio, and the y-axis indicates pathways showing a trend of enrichment. Bubble size reflects the number of genes involved in each pathway, and color intensity denotes the level of significance (*p*.adjust value).

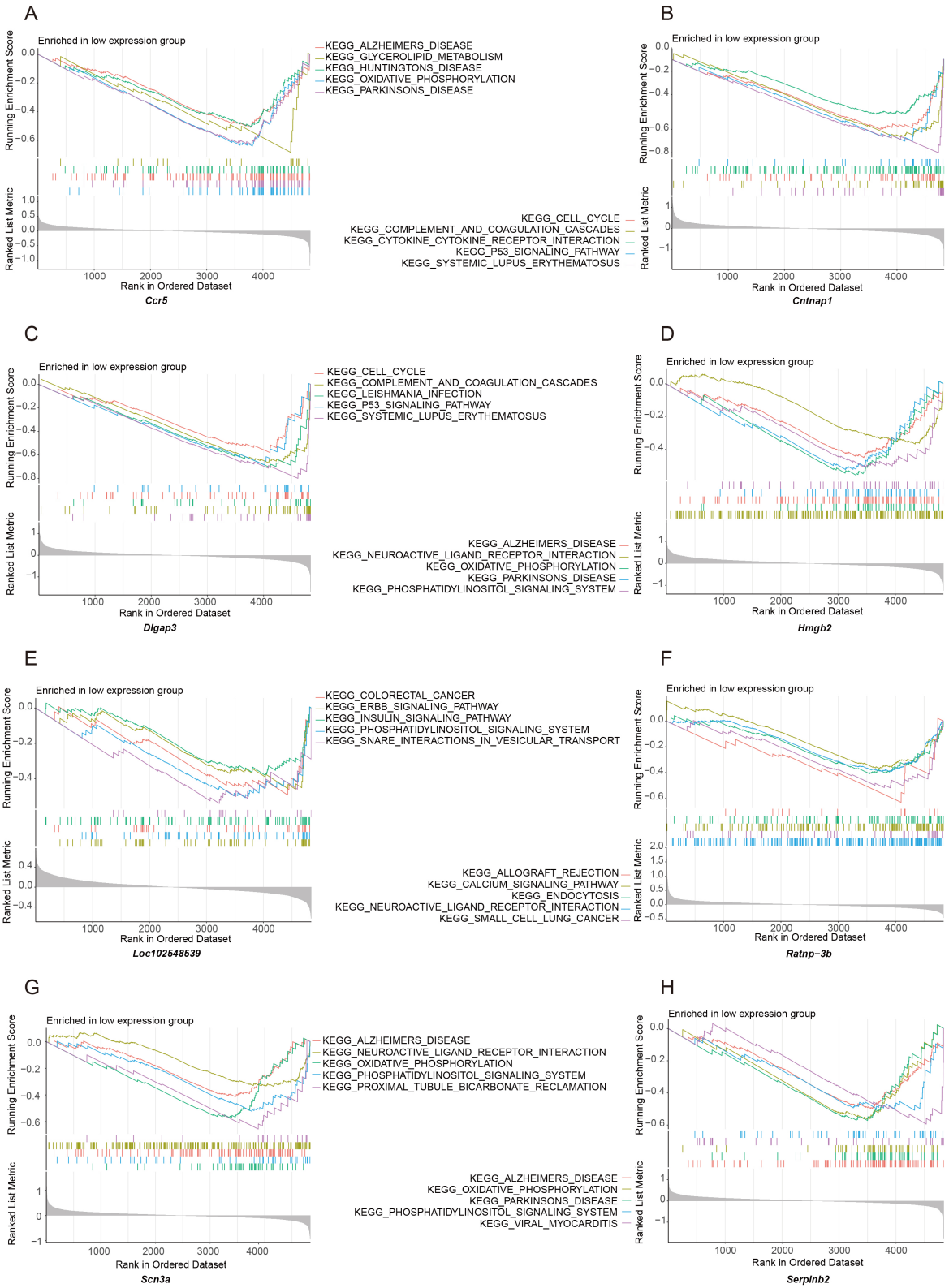

Fig. 9. Gene set enrichment analysis (GSEA) of NP key genes. (A–H) GSEA results for the eight key genes (*Ccr5, Cntnap1, Dlgap3, Hmgb2, Loc102545839, Ratnp-3b, Scn3a and Serpinb2*). In each plot, the x-axis represents the ranked position of genes across the samples, and the y-axis indicates the enrichment score (Enrichment Score, ES). The curve at the top represents the enrichment trend, and the peak position reflects the primary direction of pathway enrichment in either the high- or low-expression group.

10C), together with a reduced proportion of time spent in the open arms in the EPM (p = 0.001) (Fig. 10D). These findings suggest enhanced pain-associated anxiety-like behavior and impaired locomotor performance in SNI mice, possibly as a consequence of right hindlimb pain. RT-qPCR analysis showed that *Serpinb2* (p = 0.004) and *Scn3a* (p = 0.0444) mRNA levels were significantly higher in the ipsilateral L4–L6 DRG of SNI mice (Fig. 10E). Immunohistochemical analysis further demonstrated increased protein expression of *Serpinb2* (p = 0.0146) and *Scn3a* (p = 0.0078) in DRG neurons from the SNI group, with immunoreactivity observed mainly in neuronal profiles (Fig. 10F). Together, these findings validated the bioinformatic results at both the transcriptional and protein levels.

4. Discussion

In the present study, we performed an integrated analysis of multiple transcriptomic datasets derived from DRG tissues after peripheral nerve injury and further validated the findings with molecular and histological experiments. Our findings indicated that *Serpinb2* expression was notably increased in NP conditions, with both mRNA and protein levels significantly elevated in the DRGs of mice undergoing SNI. Immunohistochemical analysis further confirmed that *Serpinb2* remained highly expressed in the DRG. In contrast, the upregulation of *Scn3a*, a pain-related voltage-gated sodium-channel gene that has been relatively well characterized, was consistent with previous reports, and its main significance in the present study was to provide indirect support for the reliability of our integrated bioinformatic screening strategy and experimental model [18,19]. It should be noted that although *Scn9a* and *Scn10a* are generally regarded as the more classical and functionally important sodium-channel-related genes in pain research, *Scn3a* was identified through our integrative screening pipeline and was therefore included as a reference marker rather than as a primary focus of subsequent mechanistic investigation. Taken together, these findings suggested that *Serpinb2* represents a previously underappreciated but potentially important candidate molecule in the pathophysiology of NP.

The DRG is a key anatomical and functional hub in nociceptive information processing, serving as the first relay station for peripheral sensory signals before they enter the central nervous system and therefore playing an essential role in pain transmission. After peripheral-nerve injury, the DRG undergoes extensive molecular and cellular remodeling, characterized by persistent neuroinflammation, altered neuron-glia interactions, and increased excitability of primary sensory neurons [20]. Recent evidence has indicated that inflammation within the DRG is not merely a secondary consequence of nerve injury, but rather a critical driver of peripheral sensitization and pain chronification [13,21]. In this context, the significant upregulation of *Serpinb2* observed in the DRG of mice after SNI in the present study suggests that this gene may contribute to the establishment of a pro-inflammatory microenvironment, thereby supporting persistent nociceptive signaling.

Serpinb2, commonly referred to as PAI-2, belongs to the serine protease inhibitor family and has been extensively researched mainly in relation to immunity and inflammation. A previous study has shown that *Serpinb2* can be markedly induced in macrophages and monocytes under inflammatory conditions, where it participates in the regulation of immune responses, maintenance of inflammatory homeostasis, and control of cell survival [22]. In addition, *Serpinb2*-deficient models exhibited enhanced Th1-type immune responses, further supporting its role in immunoregulatory polarization [23]. More recent studies suggest that *Serpinb2* is not merely a bystander molecule accompanying inflammation, but may also contribute to macrophage metabolic adaptation, resistance to oxidative stress, and the resolution phase of inflammation, thereby influencing the stability of the local tissue microenvironment [22,24]. Although its roles in peripheral inflammation and immunity have become increasingly clear, the expression pattern and functional significance of *Serpinb2* in the nervous system remain poorly characterized. Based on currently available evidence, reports demonstrating significant upregulation of *Serpinb2* in the DRG under NP conditions remain limited, and the present study provided additional evidence supporting this observation.

From a mechanistic perspective, *Serpinb2* may not merely reflect an activated inflammatory state, but may instead be associated with multiple aspects of microenvironmental reprogramming within the DRG after nerve injury. First, as an inflammation-associated molecule, the marked upregulation of *Serpinb2* observed in the DRG in the present study suggested that it may contribute to shaping a pro-inflammatory microenvironment that supports persistent nociceptive signal transmission. Recent reports have suggested that inflammatory responses within the DRG are not simply passive consequences of nerve injury, but rather important drivers of abnormal excitability in primary sensory neurons and pain chronification; inflammatory mediators can promote aberrant nociceptive transmission by modulating ion channel activity, lowering neuronal firing thresholds, and enhancing excitatory neurotransmitter signaling [15,25,26]. In this context, the upregulation of *Serpinb2* may be associated with a pro-inflammatory state that facilitates persistent amplification of pain signaling, rather than serving merely as a bystander after injury [12,27].

Second, the DRG represents a dynamic neuroimmune unit composed of sensory neurons, satellite glial cells, resident or infiltrating immune cells, and stromal components. Studies have indicated that bidirectional communication among neurons, satellite glial cells, macrophages, and other immune cells provides an important basis for the amplification and persistence of NP [15,28]. Although the present study did not determine the precise cellular source of *Serpinb2* within the DRG, its well-established high expression

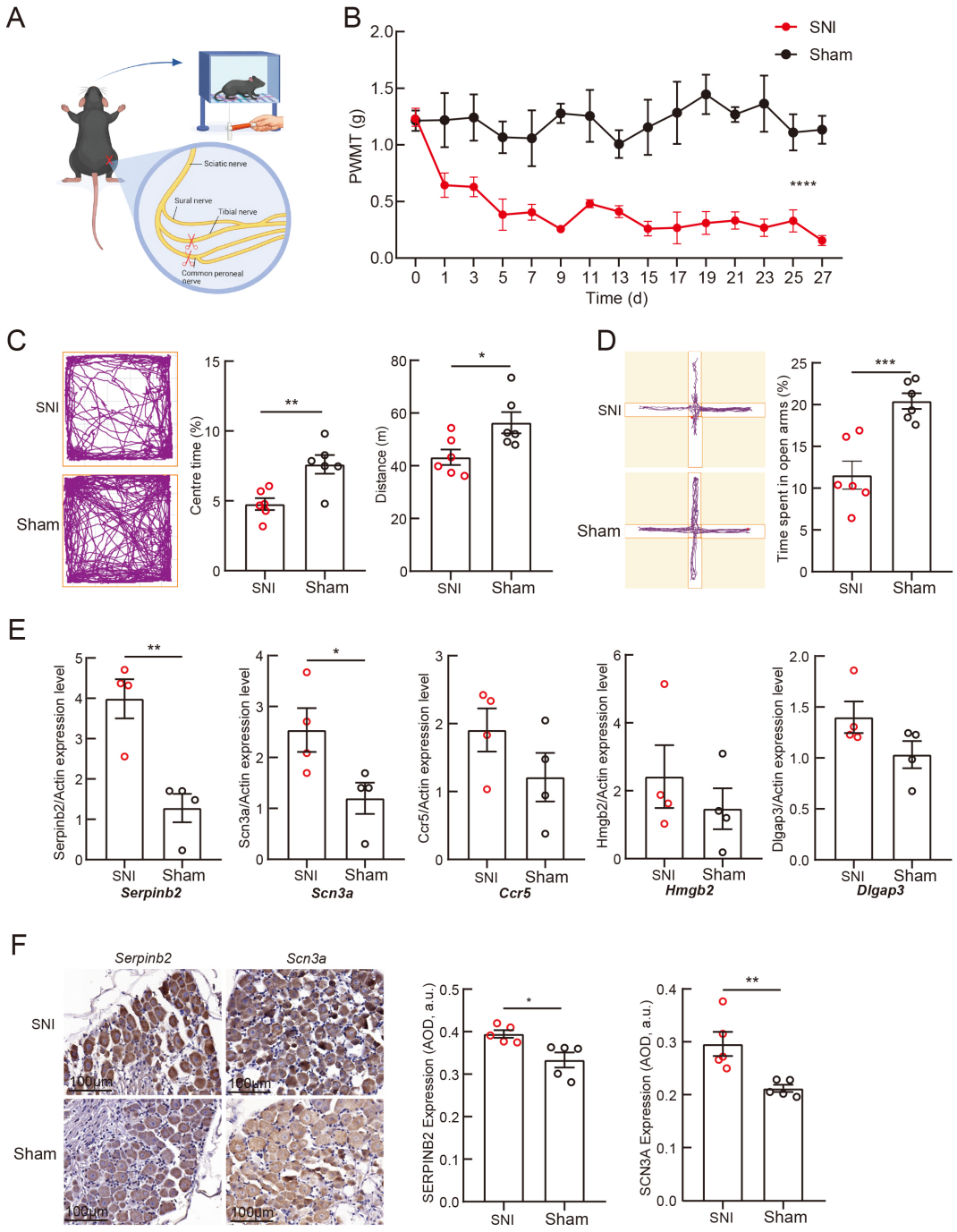

Fig. 10. Behavioral and molecular validation of NP after spared nerve injury (SNI). (A) Schematic illustration of the anatomical structure of the SNI model and the procedure for pain threshold assessment. (B) Paw withdrawal mechanical threshold (PWMT) was markedly lower in the SNI group than in the Sham group (n = 6). (C) Representative locomotor trajectories of the SNI and Sham groups in the open field test (OFT). Compared with the Sham group, mice in the SNI group showed a significantly lower percentage of time spent in the central zone and a shorter total traveling distance. (D) Representative locomotor trajectories of the SNI and Sham groups in the elevated plus maze (EPM). Mice in the SNI group spent a lower percentage of time in the open arms than those in the Sham group. (E) Bar graphs showing reverse transcription quantitative polymerase chain reaction (RT-qPCR) analysis of *Serpinb2*, *Scn3a*, *Ccr5*, *Hmgb2*, and *Dlgap3* mRNA expression levels in the DRG (n = 4). Among these genes, *Serpinb2* and *Scn3a* were upregulated in the SNI group. (F) Representative immunohistochemical staining of *Serpinb2* and *Scn3a* in the DRG from the SNI and Sham groups. The average optical density of both *Serpinb2* and *Scn3a* immunostaining was higher in the SNI group. Scale bar = 100 μm. *$p < 0.05$, **$p < 0.01$, ***$p < 0.001$, ****$p < 0.0001$.

in the monocyte-macrophage lineage suggests that it may be involved primarily in immune regulatory processes dominated by non-neuronal components. It may then indirectly influence sensory neuronal excitability through paracrine signaling, extracellular matrix alterations, or inflammatory mediator networks. In other words, *Serpinb2* may not act directly as a pro-nociceptive ion channel-related molecule, but is more likely to function as an associated component within the neuron-glia-immune cell interaction network of the DRG [27,29].

In addition, as an inhibitor of urokinase-type plasminogen activator (uPA), *Serpinb2* is closely associated with the regulation of protease activity, cell migration, extracellular matrix remodeling, and tissue repair [30]. This is particularly relevant for understanding its potential role in NP. After nerve injury, the DRG and adjacent tissues not only undergo inflammatory activation but also exhibit extracellular matrix reorganization, barrier alterations, and ongoing tissue repair, all of which are closely linked to aberrant neural plasticity and persistent sensory dysfunction [31,32]. Previous studies have suggested that *Serpinb2* can influence macrophage migratory phenotypes and matrix remodeling-related programs, and is associated with collagen remodeling, cell adhesion, and local infiltration processes [24,33]. Therefore, within the injured DRG microenvironment, *Serpinb2* may be associated with the balance between adaptive repair and maladaptive stabilization of aberrant plasticity through modulation of the uPA/protease system and its downstream matrix remodeling pathways.

The function of *Serpinb2* may also not be limited to the classical inflammation-protease axis. Previous studies have also linked *Serpinb2* to cellular stress responses, maintenance of proteostasis, and regulation of cell survival, with its expression being altered by multiple stress-related stimuli and potentially affecting cellular adaptation to proteotoxic or metabolic stress. Given that the DRG is exposed to inflammatory burden, oxidative stress, and metabolic remodeling after nerve injury, it is plausible that *Serpinb2* also participates in the maintenance of cellular homeostasis under injury conditions, thereby influencing how DRG neurons and surrounding supportive cells respond to persistent injury signals [22,34]. This possibility also provides an alternative explanation for the sustained elevation of *Serpinb2* under NP conditions: its upregulation may reflect not only pro-inflammatory amplification, but also a compensatory attempt by the tissue to limit injury progression and preserve local homeostasis.

The upregulation of *Serpinb2* observed in the present study was consistent with the emerging concept of "whole nervous system injury" in NP research [5]. This concept emphasizes the idea that peripheral-nerve injury does not merely induce local pathology, but also triggers persistent molecular remodeling across multiple levels of the peripheral sensory pathway and central pain-processing networks. As a critical interface linking peripheral injury to central sensitization, the DRG may play a pivotal role in pain chronification through injury-induced alterations in its inflammatory and immune status. Within this framework, *Serpinb2* is unlikely to be responsible for an isolated differentially expressed molecule; rather, it is more likely to constitute part of the neuroimmune-matrix remodeling network that develops in the DRG after injury. Its aberrant expression may therefore reflect the coupling among local inflammatory responses, tissue remodeling, and neuronal functional changes [20,35].

Consistent with previous studies, *Scn3a* expression was also increased in the DRG of rodents with NP [36,37]. Given that the role of voltage-gated sodium channels in regulating neuronal excitability and pain transmission has already been relatively well established, we did not pursue further mechanistic investigation of *Scn3a* in the present study. Instead, the identification of *Scn3a* primarily served to provide indirect support for the robustness of our integrated bioinformatic screening strategy and to further validate the reliability of the experimental model used in this study.

In addition to *Scn3a* and *Serpinb2*, several differentially expressed genes, including *Ccr5*, *Cntnap1*, *Dlgap3*, *Hmgb2*, *Loc102545839*, and *Ratnp-3b,* were identified between the control and NP groups. Among these, *Loc102545839* and *Ratnp-3b* remain poorly annotated and were not further validated. Although no significant differences were detected at the mRNA level for the remaining genes in RT-qPCR analyses, potential alterations at the protein or functional level cannot be excluded.

Functionally, *Scn3a, Ccr5, Cntnap1, Dlgap3* and *Hmgb2* represent key molecular nodes at distinct hierarchical levels within neuropathic pain–related networks. *Scn3a* encodes the voltage-gated sodium channel Nav1.3, which is re-expressed following nerve injury and contributes to neuronal hyperexcitability, ectopic discharges, and central sensitization [38]. *Ccr5* mediates immune cell recruitment and amplifies inflammatory responses through its ligands CCL3/CCL4/CCL5 [39]. *Hmgb2,* as a damage-associated molecular pattern (DAMP) molecule, may enhance inflammatory signaling through pathways such as nuclear factor kappa-light-chain-enhancer of activated B cells (NF-κB)/NOD-like receptor family pyrin domain containing 3 (NLRP3) and toll-like receptor 4 (TLR4)-related signaling [40]. *Cntnap1* maintains paranodal structure and regulates the spatial organization of ion channels [41], whereas *Dlgap3* governs excitatory synaptic architecture and glutamate receptor function [42].

We hypothesize that these molecules act synergistically across multiple levels along an "inflammation–excitability–structure–synaptic" axis, with *Serpinb2* potentially serving as a key regulator of the neuroinflammatory microenvironment. *Serpinb2* may functionally interact with *Ccr5* and *Hmgb2* to modulate pro-inflammatory cytokine signaling, such as interleukin-1 beta (IL-1β) and

tumor necrosis factor-alpha (TNF-α), thereby influencing the expression and function of *Scn3a*/Nav1.3 and enhancing neuronal excitability. Meanwhile, structural alterations associated with *Cntnap1* and synaptic plasticity regulated by *Dlgap3* may further amplify these processes at the circuit level.

Taken together, *Serpinb2* may contribute to the development and maintenance of neuropathic pain by modulating the neuroinflammatory microenvironment and coordinating with *Scn3a, Ccr5, Cntnap1, Dlgap3 and Hmgb2* to form a cross-level network linking inflammation, excitability, and synaptic remodeling. Notably, the identification of *Serpinb2* extends the focus from classical excitability-related mechanisms to neuroimmune regulation and microenvironmental remodeling within the DRG, thereby providing a novel perspective on the peripheral mechanisms of NP. Given the complexity and incomplete understanding of NP, this integrative framework offers a more systematic explanation for persistent hyperexcitability and highlights inflammation, ion channel function, and synaptic stability as potentially coupled therapeutic targets involved in the pathogenesis and persistence of NP.

Nevertheless, certain limitations of this study should be acknowledged. First, the current findings were largely correlative. Although *Serpinb2* showed persistent upregulation across multiple transcriptomic datasets and this observation was further validated by molecular and histological experiments, functional-loss and gain-of-function studies are still required to determine whether *Serpinb2* plays a causal role in NP behaviors and DRG neuroinflammation. Second, the cell-type-specific localization of *Serpinb2* within the DRG remains to be clarified, particularly with respect to different sensory neuron subpopulations, satellite glial cells, and infiltrating immune cells. Third, the present study focused primarily on a single peripheral-nerve-injury model; further validation in additional NP models and across different species will be necessary to assess the generalizability and robustness of these findings. Future studies should also investigate whether modulation of *Serpinb2* alters the expression of pain-related ion channels and pro-inflammatory cytokines in the DRG, such as *Scn3a*, TNF-α, and IL-1β, thereby providing deeper mechanistic insight into its potential role in NP.

5. Conclusions

Through integrated transcriptomic analysis and experimental validation, this study identified *Serpinb2* as a significantly upregulated gene in the DRG under NP conditions. The findings suggested that *Serpinb2* may be associated with neuroinflammatory regulation and microenvironmental remodeling after nerve injury. These results suggested that *Serpinb2* is a potentially important but previously underappreciated molecule in the peripheral mechanisms of neuropathic pain.

Availability of Data and Materials

The transcriptomic datasets analyzed in this study were downloaded from the GEO database under accession numbers GSE24982, GSE30691, and GSE63442. The datasets generated and analyzed during the current study are available from the corresponding author on reasonable request.

Author Contributions

DZ performed the data analysis and visualization and conducted the immunohistochemistry and quantitative PCR experiments. ZJ established the mouse SNI model and performed dorsal root ganglion tissue collection. DZ and ZJ cowrote the first draft. AZ and XZ carried out the behavioral assessments. EL conceived the study and reviewed the manuscript. All authors contributed to editorial changes in the manuscript. All authors read and approved the final manuscript. All authors have participated sufficiently in the work and agreed to be accountable for all aspects of the work.

Ethics Approval and Consent to Participate

All animal-related procedures were approved by the Institutional Animal Ethics Committee of Nanchang University (Ethics approval No. CDYFY-IACUC-202505GR037) and carried out in accordance with the institutional regulations on the care and use of laboratory animals of Nanchang University.

Acknowledgment

We gratefully acknowledge the Jiangxi Provincial Mental Health Center Biopsychiatric Laboratory for providing experimental facilities and technical support.

Funding

This research received no external funding.

Conflicts of Interest

The authors declare no conflicts of interest.

Declaration of AI and AI-Assisted Technologies in the Writing Process

In the course of preparing this manuscript, ChatGPT-3.5 was used solely for language assistance, specifically for spelling and grammar checking. The authors carefully reviewed and edited the text after using this tool and assume full responsibility for all content presented in the final publication.

Supplementary Material

Supplementary material associated with this article can be found, in the online version, at https://doi.org/10.31083/JIN50669.

References

[1] Cohen SP, Vase L, Hooten WM. Chronic pain: an update on burden, best practices, and new advances. Lancet (London, England). 2021; 397: 2082–2097. https://doi.org/10.1016/S0140-6736(21)00393-7

[2] Naranjo C, Del Reguero L, Moratalla G, Hercberg M, Valenzuela M, Failde I. Anxiety, depression and sleep disorders in patients with diabetic neuropathic pain: a systematic review. Expert Review of Neurotherapeutics. 2019; 19: 1201–1209. https://doi.org/10.1080/14737175.2019.1653760

[3] Cherif F, Zouari HG, Cherif W, Hadded M, Cheour M, Damak R. Depression Prevalence in Neuropathic Pain and Its Impact on the Quality of Life. Pain Research & Management. 2020; 2020: 1–8. https://doi.org/10.1155/2020/7408508

[4] Lin XH, Jiang R, Huang CS, Chen XW. Application and Therapeutic Mechanisms of Non-pharmacological Interventions in The Management of Chronic Pain. Progress in Biochemistry and Biophysics. 2023; 50: 2406–2419. https://doi.org/10.16476/j.pibb.2023.0293 (In Chinese).

[5] An JX, Zhang JF. A New theory of peripheral neuropathic pain: Total nerve injury. Chinese Journal of Pain Medicine. 2022; 9: 724–732. https://doi.org/10.3969/j.issn.1006-9852.2022.10.002 (In Chinese).

[6] Girgis FL, Parry CB. Management of causalgia after peripheral nerve injury. International Disability Studies. 1989; 11: 15–20. https://doi.org/10.3109/02599148909166371

[7] West SJ, Bannister K, Dickenson AH, Bennett DL. Circuitry and plasticity of the dorsal horn–toward a better understanding of neuropathic pain. Neuroscience. 2015; 300: 254–275. https://doi.org/10.1016/j.neuroscience.2015.05.020

[8] Bai YW, Yang QH, Chen PJ, Wang XQ. Repetitive transcranial magnetic stimulation regulates neuroinflammation in neuropathic pain. Frontiers in Immunology. 2023; 14: 1172293. https://doi.org/10.3389/fimmu.2023.1172293

[9] Tung KW, Behera D, Biswal S. Neuropathic pain mechanisms and imaging. Seminars in Musculoskeletal Radiology. 2015; 19: 103–111. https://doi.org/10.1055/s-0035-1547371

[10] Rosner J, de Andrade DC, Davis KD, Gustin SM, Kramer JLK, Seal RP, et al. Central neuropathic pain. Nature Reviews. Disease Primers. 2023; 9: 73. https://doi.org/10.1038/s41572-023-00484-9

[11] Felix R, Corzo-Lopez A, Sandoval A. Voltage-Gated Ion Channels in Neuropathic Pain Signaling. Life (Basel, Switzerland). 2025; 15: 888. https://doi.org/10.3390/life15060888

[12] Jang K, Garraway SM. A review of dorsal root ganglia and primary sensory neuron plasticity mediating inflammatory and chronic neuropathic pain. Neurobiology of Pain (Cambridge, Mass.). 2024; 15: 100151. https://doi.org/10.1016/j.ynpai.2024.100151

[13] Banh C, Sic A, Knezevic NN. Sodium Channel Inhibitors in Clinical Development for Pain Management: A Focused Review. CNS Drugs. 2026; 40: 165–180. https://doi.org/10.1007/s40263-025-01244-x

[14] Decosterd I, Woolf CJ. Spared nerve injury: an animal model of persistent peripheral neuropathic pain. Pain. 2000; 87: 149–158. https://doi.org/10.1016/S0304-3959(00)00276-1

[15] Ahlgreen OA, Hansen MW, Baake J, Hybel TE, Rossi R, Lai X, et al. Mapping Satellite Glial Cell Heterogeneity Reveals Distinct Spatial Organization and Implies Functional Diversity in the Dorsal Root Ganglion. Advanced Science (Weinheim, Baden-Wurttemberg, Germany). 2026; 13: e11569. https://doi.org/10.1002/advs.202511569

[16] Chaplan SR, Bach FW, Pogrel JW, Chung JM, Yaksh TL. Quantitative assessment of tactile allodynia in the rat paw. Journal of Neuroscience Methods. 1994; 53: 55–63. https://doi.org/10.1016/0165-0270(94)90144-9

[17] Dixon WJ. Efficient analysis of experimental observations. Annual Review of Pharmacology and Toxicology. 1980; 20: 441–462. https://doi.org/10.1146/annurev.pa.20.040180.002301

[18] He XH, Zang Y, Chen X, Pang RP, Xu JT, Zhou X, et al. TNF-α contributes to up-regulation of Nav1.3 and Nav1.8 in DRG neurons following motor fiber injury. Pain. 2010; 151: 266–279. https://doi.org/10.1016/j.pain.2010.06.005

[19] Tan AM, Samad OA, Dib-Hajj SD, Waxman SG. Virus-Mediated Knockdown of Nav1.3 in Dorsal Root Ganglia of STZ-Induced Diabetic Rats Alleviates Tactile Allodynia. Molecular Medicine (Cambridge, Mass.). 2015; 21: 544–552. https://doi.org/10.2119/molmed.2015.00063

[20] da Silva MDV, Martelossi-Cebinelli G, Yaekashi KM, Carvalho TT, Borghi SM, Casagrande R, et al. A Narrative Review of the Dorsal Root Ganglia and Spinal Cord Mechanisms of Action of Neuromodulation Therapies in Neuropathic Pain. Brain Sciences. 2024; 14: 589. https://doi.org/10.3390/brainsci14060589

[21] Qu Y, Cai R, Li Q, Wang H, Lu L. Neuroinflammation signatures in dorsal root ganglia following chronic constriction injury. Heliyon. 2024; 10: e31481. https://doi.org/10.1016/j.heliyon.2024.e31481

[22] Vasamsetti SB, Sadaf S, Uddin MA, Shen J, Johny E, Mondal A, et al. Tissue-resident macrophage survival depends on mitochondrial function regulated by SerpinB2 in chronic inflammation. Nature Communications. 2026; 17: 1493. https://doi.org/10.1038/s41467-026-69196-4

[23] Schroder WA, Gardner J, Le TT, Duke M, Burke ML, Jones MK, et al. SerpinB2 deficiency modulates Th1/Th2 responses after schistosome infection. Parasite Immunology. 2010; 32: 764–768. https://doi.org/10.1111/j.1365-3024.2010.01241.x

[24] Janciauskiene S, Lechowicz U, Pelc M, Olejnicka B, Chorostowska-Wynimko J. Diagnostic and therapeutic value of human serpin family proteins. Biomedicine & Pharmacotherapy = Biomedecine & Pharmacotherapie. 2024; 175: 116618. https://doi.org/10.1016/j.biopha.2024.116618

[25] Basbaum AI, Bautista DM, Scherrer G, Julius D. Cellular and molecular mechanisms of pain. Cell. 2009; 139: 267–284. https://doi.org/10.1016/j.cell.2009.09.028

[26] Xia Y, Cai M, Zhou Y, Yao Y, Jiang M, Gu D, et al. Immune Cell Biology in Peripheral Nervous System Injury. Neurorehabilitation and Neural Repair. 2025; 39: 230–240. https://doi.org/10.1177/15459683241304325

[27] Jain A, Gyori BM, Hakim S, Jain A, Sun L, Petrova V, et al. Nociceptor-immune interactomes reveal insult-specific immune signatures of pain. Nature Immunology. 2024; 25: 1296–1305. https://doi.org/10.1038/s41590-024-01857-2

[28] Bercik P. Purinergic Pathways in the Spinal Microglia as a Putative Target for Treatment of Chronic Abdominal Pain. Cellular and Molecular Gastroenterology and Hepatology. 2022; 13: 1257–1258. https://doi.org/10.1016/j.jcmgh.2021.12.016

[29] Qiu X, Yang Y, Da X, Wang Y, Chen Z, Xu C. Satellite glial cells in sensory ganglia play a wider role in chronic pain via multiple mechanisms. Neural Regeneration Research. 2024; 19: 1056–1063. https://doi.org/10.4103/1673-5374.382986

[30] Kanno Y. The uPA/uPAR System Orchestrates the Inflammatory Response, Vascular Homeostasis, and Immune System in Fibrosis Progression. International Journal of Molecular Sciences. 2023; 24: 1796. https://doi.org/10.3390/ijms24021796

[31] Tajerian M, Clark JD. The role of the extracellular matrix in chronic pain following injury. Pain. 2015; 156: 366–370. https://doi.org/10.1097/01.j.pain.0000460323.80020.9d

[32] Metafune M, Muratori L, Fregnan F, Ronchi G, Raimondo S. The extracellular matrix in peripheral nerve repair and regeneration: a narrative review of its role and therapeutic potential. Frontiers in Neuroanatomy. 2025; 19: 1628081. https://doi.org/10.3389/fnana.2025.1628081

[33] Song Q, E S, Zhang Z, Liang Y. Neuroplasticity in the transition from acute to chronic pain. Neurotherapeutics : the Journal of the American Society for Experimental NeuroTherapeutics. 2024; 21: e00464. https://doi.org/10.1016/j.neurot.2024.e00464

[34] Lee JA, Yerbury JJ, Farrawell N, Shearer RF, Constantinescu P, Hatters DM, et al. SerpinB2 (PAI-2) Modulates Proteostasis via Binding Misfolded Proteins and Promotion of Cytoprotective Inclusion Formation. PloS One. 2015; 10: e0130136. https://doi.org/10.1371/journal.pone.0130136

[35] Dong FL, Yu L, Feng PD, Ren JX, Bai XH, Lin JQ, et al. An atlas of neuropathic pain-associated molecular pathological characteristics in the mouse spinal cord. Communications Biology. 2025; 8: 70. https://doi.org/10.1038/s42003-025-07506-0

[36] Lindia JA, Köhler MG, Martin WJ, Abbadie C. Relationship between sodium channel NaV1.3 expression and neuropathic pain behavior in rats. Pain. 2005; 117: 145–153. https://doi.org/10.1016/j.pain.2005.05.027

[37] Lai J, Hunter JC, Porreca F. The role of voltage-gated sodium channels in neuropathic pain. Current Opinion in Neurobiology. 2003; 13: 291–297. https://doi.org/10.1016/s0959-4388(03)00074-6

[38] Hains BC, Klein JP, Saab CY, Craner MJ, Black JA, Waxman SG. Upregulation of sodium channel Nav1.3 and functional involvement in neuronal hyperexcitability associated with central neuropathic pain after spinal cord injury. The Journal of Neuroscience : the Official Journal of the Society for Neuroscience. 2003; 23: 8881–8892. https://doi.org/10.1523/JNEUROSCI.23-26-08881.2003

[39] Ishida Y, Kimura A, Kuninaka Y, Inui M, Matsushima K, Mukaida N, et al. Pivotal role of the CCL5/CCR5 interaction for recruitment of endothelial progenitor cells in mouse wound healing. The Journal of Clinical Investigation. 2012; 122: 711–721. https://doi.org/10.1172/JCI43027

[40] Zhang Y, Zhao Z, Zhao X, Xie H, Zhang C, Sun X, et al. HMGB2 causes photoreceptor death via down-regulating Nrf2/HO-1 and up-regulating NF-κB/NLRP3 signaling pathways in light-induced retinal degeneration model. Free Radical Biology & Medicine. 2022; 181: 14–28. https://doi.org/10.1016/j.freeradbiomed.2022.01.018

[41] Chang C, Sell LB, Shi Q, Bhat MA. Mouse models of human CNTNAP1-associated congenital hypomyelinating neuropathy and genetic restoration of murine neurological deficits. Cell Reports. 2023; 42: 113274. https://doi.org/10.1016/j.celrep.2023.113274

[42] Rasmussen AH, Rasmussen HB, Silahtaroglu A. The DLGAP family: neuronal expression, function and role in brain disorders. Molecular Brain. 2017; 10: 43. https://doi.org/10.1186/s13041-017-0324-9